Journal of Molecular Liquids 380 (2023) 121758

Contents lists available at ScienceDirect

Journal of Molecular Liquids

journal homepage: www.elsevier.com/locate/molliq

Acidochromism of amino-substituted indolizine chromophores: Towards white light emission

Teresa Antón-Cánovas [a], Sylvain Achelle [b], M. Paz Fernández-Liencres [c], Amparo Navarro [c], Francisco Alonso [a,*], Julián Rodríguez-López [d,*]

[a] Universidad de Alicante, Instituto de Síntesis Orgánica (ISO) and Departamento de Química Orgánica, Facultad de Ciencias, Apdo. 99, 03080 Alicante, Spain
[b] Univ. Rennes, CNRS, Institut des Sciences Chimiques de Rennes (ISCR), UMR 6226, F-35000 Rennes, France
[c] Universidad de Jaén, Departamento de Química Física y Analítica, Facultad de Ciencias Experimentales, Campus Las Lagunillas, 23071 Jaén, Spain
[d] Universidad de Castilla-La Mancha, Área de Química Orgánica, Facultad de Ciencias y Tecnologías Químicas, Avda. Camilo José Cela 10, 13071 Ciudad Real, Spain

ARTICLE INFO

Article history:
Received 8 January 2023
Revised 24 February 2023
Accepted 28 March 2023
Available online 2 April 2023

Keywords:
Indolizines
Photophysical properties
Fluorescence
DFT calculations

ABSTRACT

There is a continuous interest in the development of advanced materials with tunable photophysical properties, among which white light emission represents a major challenge. Indolizines are a kind of aza-heterocycles that have gained a great deal of attention in the recent past due to their intriguing photophysical behavior. We report herein on the synthesis of new push–pull indolizines bearing amino and electron-withdrawing groups at positions 1 and 7, respectively, and on their optical response in acidic medium. Exclusive protonation on the amino group has led to a hypsochromic shift in the emission spectra. Interestingly, white photoluminescence can be attained by adjusting the amount of acid as a result of color complementarity between neutral and charged species. Moreover, Density Functional Theory (DFT) calculations on the molecular structure and photophysical properties of these compounds are in agreement with the experimental results, providing very useful information about the main electronic transitions and the influence of protonation on the optical transitions.

1. Introduction

In the last years, organic push–pull chromophores with extended π-conjugated structure have been intensively studied due to their promising optoelectronic properties [1,2]. In this context, π-deficient azaheterocycles have been widely used as moderate-to-strong electron-withdrawing groups. In such cases, some molecules proved to be highly sensible to environmental stimuli. In addition to polarity, the presence of acids, metal cations, or diverse biomolecules can induce substantial changes in the photophysical properties due to the potential for protonation, complexation, and hydrogen bonding with the nitrogen atoms, which increases the electron-withdrawing character and the intramolecular charge transfer [3]. This phenomenon has enabled the development of a broad variety of new sensors and optical switches. On the other hand, there is a general upsurge of interest in the development of white light emitting materials which, although challenging, when incorporated into proper devices can find multiple and appealing applications in a variety of fields [4].

Indolizines are nitrogen-fused bicyclic heteroaromatic compounds containing both π-rich and π-deficient five- and six-membered rings [5,6], respectively, which are very attractive scaffolds in materials science because of their diverse and useful applications. For instance, materials based on indolizine dyes have been applied in laser-based reading and recording devices [7], optical filters [8], thermography and photothermography [7a], electrochromic devices [9], and photoelectric converters [10]. Particularly, the past decade has witnessed a growing interest in the photophysical properties of indolizines, because those featuring fluorescent character (Fig. 1, **I**-**VI**) [11] can exhibit a great potential in the field of sensors and bioimaging [12].

The indolizine nucleus turned out to be a strong electron-donating group that contributes to electron density more significantly than the commonly employed arylamine-based donors. This fact can be rationalized through several factors, including the planarization of the nitrogen atom, the reduced charge-transfer energy barriers to access the excited state by generation of a stabilized aromatic pyridinium upon light absorption, and the good directionality of the electron donation [13].

* Corresponding authors.
E-mail addresses: falonso@ua.es (F. Alonso), julian.rodriguez@uclm.es (J. Rodríguez-López).

https://doi.org/10.1016/j.molliq.2023.121758
0167-7322/

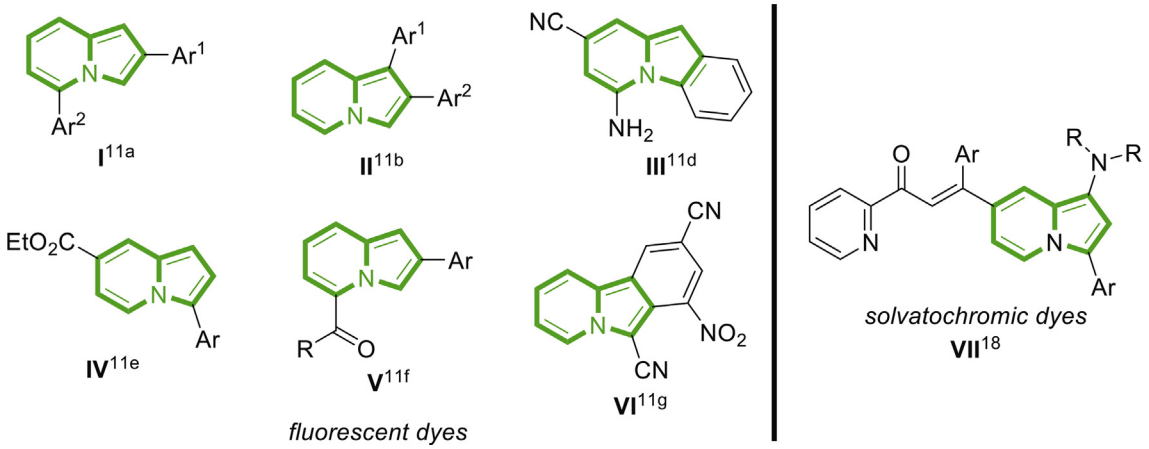

Fig. 1. Structure of indolizines showing prominent photophysical properties.

For the vast majority of conjugated push–pull molecules based on π-deficient azaheterocycles, protonation involves enhanced intramolecular charge transfer (ICT) and red-shifting of the ICT absorption and emission curves [3,14]. In contrast, protonation of indolizine decreases its electron-donating character, leading to a hypsochromic (blue) shift. Indolizine is exclusively protonated at 3-position, giving a pyridinium salt (pK_a = 3.9) [15], but the protonation of pH-responsive groups introduced at specific positions in accordance with their pK_a values allows to control the direction of the emission shift and the desired emission color [16]. In some cases, a blue shift in emission upon protonation is desirable.

Our ongoing interest on the photophysical properties of heterocyclic compounds [3] and on the reactivity of 1-amino indolizines [17] has led to the discovery of a new family of indolizine dyes with solvatochromic properties and application in plastic coloration (Fig. 1, **VII**) [18]. In this context, we describe herein the synthesis of a new family of 3-arylindolizine derivatives bearing tertiary amino groups at 1-position as pH-responsive elements and electron-withdrawing moieties at 7-position. Protonation of the amino groups reduces the electron-donating character and prompts the appearance of hypsochromically shifted emission bands of complementary colors. White photoluminescence can be obtained by an accurate control of the amount of acid added. The molecular structure and photophysical properties of this new family of compounds have been characterized by Density Functional Theory (DFT) at the M06-2X/6–31+G** level of theory. The theoretical insights have allowed us to deepen into the nature of the main electronic transitions observed in the experimental spectra and the impact of protonation on the different optical transitions.

2. Results and discussion

2.1. Synthesis of indolizines

All the indolizines in this study were previously synthesized by some of us. The starting indolizines **1** were obtained according to a three-component reaction of pyridine-2-carbaldehyde, a secondary amine, and a terminal alkyne, catalyzed by copper nanoparticles supported on activated carbon (CuNPs/C) (Scheme 1a) [19]. These indolizines were subjected to a novel formylation method, based on the use of the Eschenmoser's salt in the presence of a base at room temperature (Scheme 1b) [20]. The corresponding indolizinecarbaldehydes **2** were obtained in moderate yields. Finally, the π-conjugation of the indolizine **2a** was extended through a mono-condensation reaction with acetone. The expected product **3a** was obtained in almost quantitative yield under standard conditions (Scheme 1c) [20].

2.2. Photophysical properties

Table 1 summarizes the absorption and emission data for compound **2** and **3**, registered in CH_2Cl_2 at room temperature (see Figs. S1-S4 in the Supplementary data). All the compounds absorbed light in the blue region of the spectrum (more intense bands of higher energy were also observed) and showed a typical orange-red emission when irradiated (597–657 nm). Compared to **2a-c**, compound **3a** exhibited the most red-shifted spectra due to its extended conjugation. In general, large Stokes shifts occurred in all cases. Although many indolizine derivatives show relatively low stability under ambient conditions, blocking the most reactive positions 1 and 3 of the indolizine nucleus can provide more stable compounds [21]. In our case, all compounds were thermally and photochemically stable over the experimentation span, and did not undergo changes in the emission intensity after continuous irradiation for 1000 s (Figs. S5-S8).

In addition, the emission maxima showed a significant solvent dependence. Thus, a positive solvatochromism was observed in all cases when the polarity of the solvent was increased, which is characteristic of chromophores that experience an intramolecular charge transfer (ICT) upon excitation (Fig. 2, Table S1 and Figs. S9-11) [23].

The molecular structure and photophysical properties of **2a-c** and **3a** were optimized at the TD-M06-2X/6–31+G** level of theory in CH_2Cl_2 solution to characterize the electronic transitions involved in the experimental absorption and emission spectra (see Computational details in the Experimental Section). The vertical electronic transitions calculated for these compounds collected in Table 2 are in good agreement with the experimental absorption wavelengths (differences < 0.14 eV). As observed experimentally, the most red-shifted transition is predicted for compound **3a** in accordance with the more extended π-conjugation. For all compounds, the lowest energy electronic transition $S_0 \rightarrow S_1$ shows a high contribution HOMO → LUMO, and therefore charge transfer character. Fig. 3 shows a representation of the frontier molecular orbitals. The HOMO is spread over the amino group and the indolizine nucleus, while the LUMO is mainly located on the indolizine, showing in both cases a low participation of the aryl ring.

The large Stokes shifts observed for these compounds in solution could be justified on the basis of significant changes in the molecular geometry when the molecule is photoexcited. Fig. 4 shows some selected dihedral angles predicted for the ground

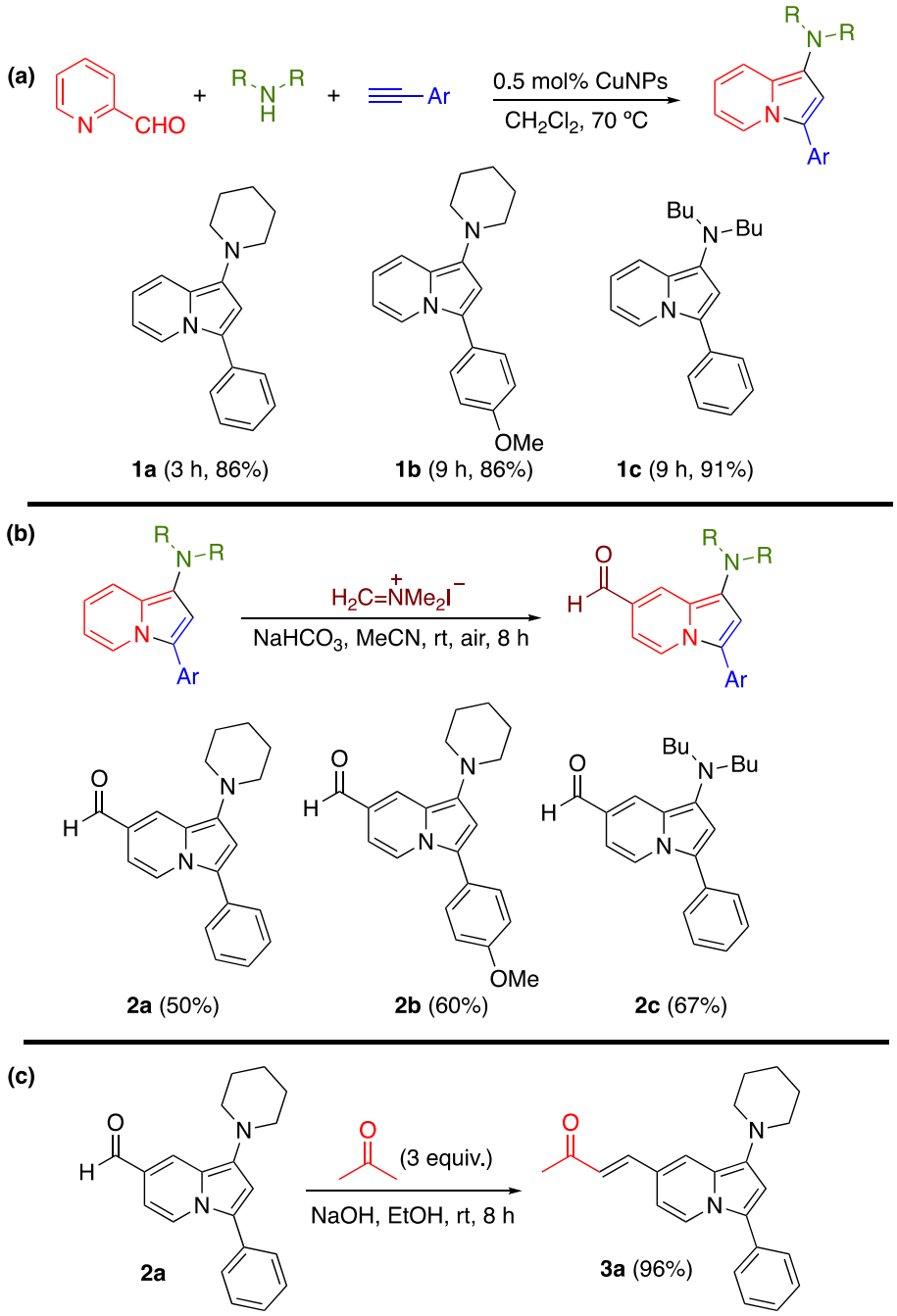

Scheme 1. (a) Synthesis of the starting indolizines **1**. (b) Formylation of the indolizines **1** with the Eschenmoser's salt. (c) Synthesis of the π-extended indolizine **3a**.

Table 1
Photophysical properties of compounds **2** and **3** in CH_2Cl_2 and acidified CH_2Cl_2 (10^{-2} M TFA)[a].

Compd	CH_2Cl_2			CH_2Cl_2 + TFA		
	λ_{abs} [nm] (ε [$mM^{-1}·cm^{-1}$])	λ_{em} [nm][b] (ϕ_F[c])	Stokes shift [cm^{-1}][d]	λ_{abs} [nm] (ε [$mM^{-1}·cm^{-1}$])	λ_{em} [nm][b] (ϕ_F[c])	Stokes shift [cm^{-1}][d]
2a	304 (20.2), 375 (3.7), 449 (8.1)	604 (0.06)	5715	273 (27.0), 330 (5.8), 384 (8.6)	480 (0.15)	5208
2b	307 (18.7), 371 (3.8), 450 (8.3)	607 (0.04)	5748	275 (16.4), 334 (3.1), 391 (6.3)	491 (0.07)	5209
2c	311 (20.1), 455 (8.2)	597 (0.06)	5227	272 (30.7), 325 (7.6), 382 (11.1)	476 (0.34)	5169
3a	318 (7.7), 478 (5.6)	657 (0.06)	5700	289 (6.5), 411 (4.5), 583 (0.7)	503 (0.08)	4450[e]

[a] All spectra were registered at room temperature (c = 1.0–3.0 × 10^{-6} M). [b] Excitation at the lowest energy absorption band. [c] Fluorescence quantum yield determined relative to that of 9,10-bis(phenylethynyl)anthracene in cyclohexane (ϕ_F = 1) [22]. [d] Stokes shift calculated using the absorption band of lowest energy. [e] Calculated using the absorption band at 411 nm.

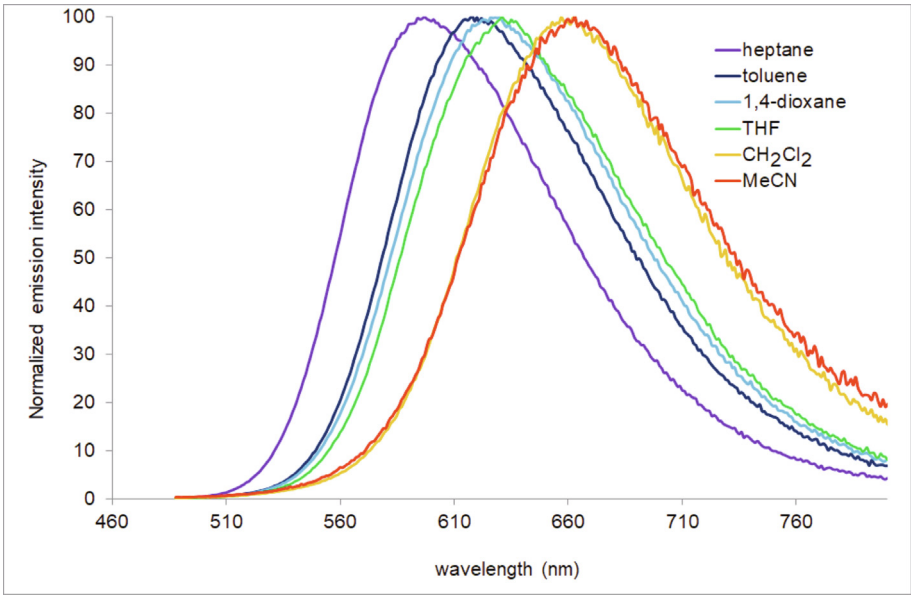

Fig. 2. Normalized emission spectra of **3a** in various solvents of different polarity ($c \cong 10^{-5}$ M, λ_{exc} = 478 nm).

Table 2
Experimental maximum absorption wavelength (λ_{ab}^{exp}) and calculated vertical electronic transitions (λ_{ab}^{calc}), oscillator strength (*f*), and main components of the $S_0 \rightarrow S_n$ transition (% contribution) at the TD-M062X/6–31+G** level of theory in CH_2Cl_2 solution.

Compd	λ_{ab}^{exp} eV(nm)	λ_{ab}^{calc} eV (nm)	Transition	*f*	% Contribution
2a	2.76 (449)	2.63 (472)3.79	$S_0 \rightarrow S_1$	0.27	H → L (95)
		(327)	$S_0 \rightarrow S_2$	0.17	H → L + 1 (69)
		4.32 (287)	$S_0 \rightarrow S_5$	0.50	H-1 → L (60), H → L + 1 (16)
2b	2.76 (450)	2.62 (473)3.85	$S_0 \rightarrow S_1$	0.27	H → L (95)
		(322)4.33	$S_0 \rightarrow S_3$	0.18	H-5 → L (75)
		(287)	$S_0 \rightarrow S_5$	0.83	H-1 → L (69), H → L + 2 (10)
2c	2.72 (455)	2.78 (445)3.97	$S_0 \rightarrow S_1$	0.25	H → L (95)
		(313)4.36	$S_0 \rightarrow S_3$	0.14	H → L + 1 (69), H → H-1 → L (11)
		(284)	$S_0 \rightarrow S_4$	0.51	H-1 → L (62), H → L + 1 (19)
3a	2.59 (478)	2.55 (485)3.56	$S_0 \rightarrow S_1$	0.71	H → L (94)
		(348)4.13	$S_0 \rightarrow S_2$	0.22	H → L + 1 (50), H → L + 2 (37)
		(301)	$S_0 \rightarrow S_5$	0.58	H-1 → L (67), H → L + 1 (16)
			+ TFA		
2aH$^+$	3.23 (384)	3.37 (368)4.01	$S_0 \rightarrow S_1$	0.26	H → L (95)
		(309)5.33	$S_0 \rightarrow S_4$	0.83	H-1 → L (47), H → L + 1 (39)
		(233)	$S_0 \rightarrow S_7$	0.22	H → L + 3 (38), H → L + 5 (27), H → L + 4 (11)
2bH$^+$	3.17 (391)	3.32 (374)4.74	$S_0 \rightarrow S_1$	0.27	H → L (92)
		(261)5.16	$S_0 \rightarrow S_4$	0.78	H-1 → L (50), H → L + 1 (34)
		(240)	$S_0 \rightarrow S_6$	0.20	H-3 → L (24), H-1 → L (21), H-2 → L (12), H → L + 2 (12)
2cH$^+$	3.25 (382)	3.34 (369)4.30	$S_0 \rightarrow S_1$	0.25	H → L (96)
		(255)4.61	$S_0 \rightarrow S_4$	0.82	H-1 → L (45), H → L + 1 (42)
		(233)	$S_0 \rightarrow S_6$	0.11	H → L + 3 (38), H → L + 2 (24), H-5 → L (20)
3aH$^+$	3.02 (411)	3.34 (371)4.30	$S_0 \rightarrow S_1$	0.74	H → L (94)
		(288)	$S_0 \rightarrow S_3$	0.16	H → L + 1 (81), H-1 → L (10)
		4.61 (269)	$S_0 \rightarrow S_4$	0.51	H-1 → L (59), H-3 → L (21)

and first excited state. Large values are predicted for the dihedral angle τ_1 between the amino group and the indolizine nucleus, which decreases between 17 and 28° upon photoexcitation. The variations of the dihedral angles τ_2, τ_3, and τ_4 are much smaller.

According to previous studies [24], stable conformations may be obtained in the excited state by a twisted intramolecular charge transfer (TICT) process. In the TICT state, the amino group twists out the central nucleus by almost 90° upon photoexcitation. In alternative to the TICT process, the photoexcitation may cause a decrease in the dihedral angle, as occurs in the systems studied in this work, generating a more planar conformation in the excited state through a planar intramolecular charge transfer (PICT) pathway [25]. In the case of polar solvents, the resulting charge separation would be stabilized, giving rise to dark states in solution. For nonpolar solvents, the emission arises from the so-called locally excited state (LE), whose geometry is usually similar to that of the ground state, yielding bright states upon excitation.

By studying systems in which charge transfer states can be stabilized after photoexcitation, it has been shown that the relative stabilization of the LE and ICT (TICT or PICT) states depends on the functional used to calculate the S_1 potential energy surface (PES) profile [25,26]. Therefore, global hybrid functionals with high fraction of Hartree-Fock exchange such as M06-2X (HF = 54%) and range-separated functionals are recommended to avoid computational artifacts and achieve good agreement with experimental data. In addition, the methodology chosen to describe the solvation as linear response (LR), corrected linear- response (cLR), or state-specific (SS) is also crucial for a correct description of the S_1 PES

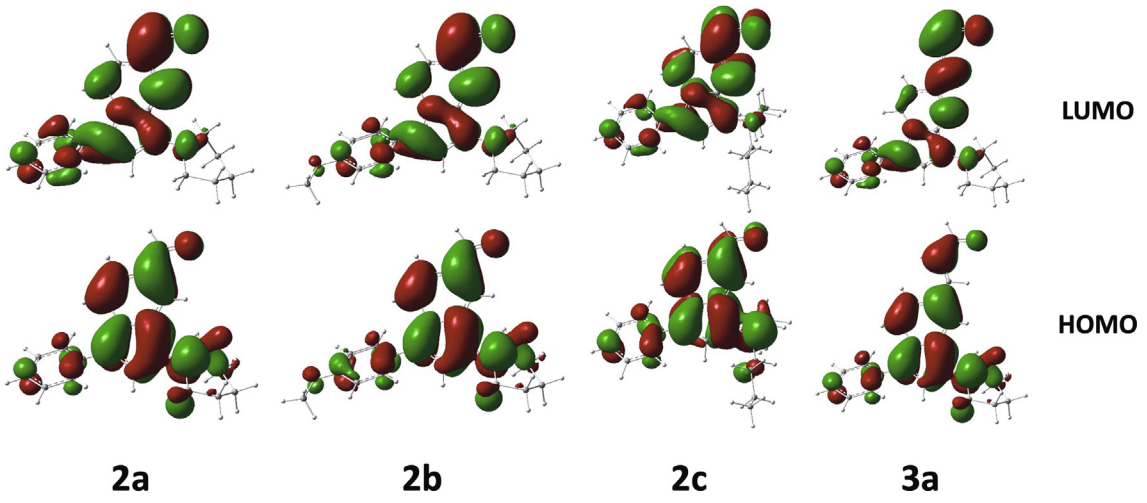

Fig. 3. HOMO and LUMO molecular orbitals (isocontour plots 0.02 a.u.) calculated for **2a, 2b, 2c,** and **3a** at the M06-2X/6–31+G** level of theory in CH_2Cl_2 solution (see energy levels in Table S2).

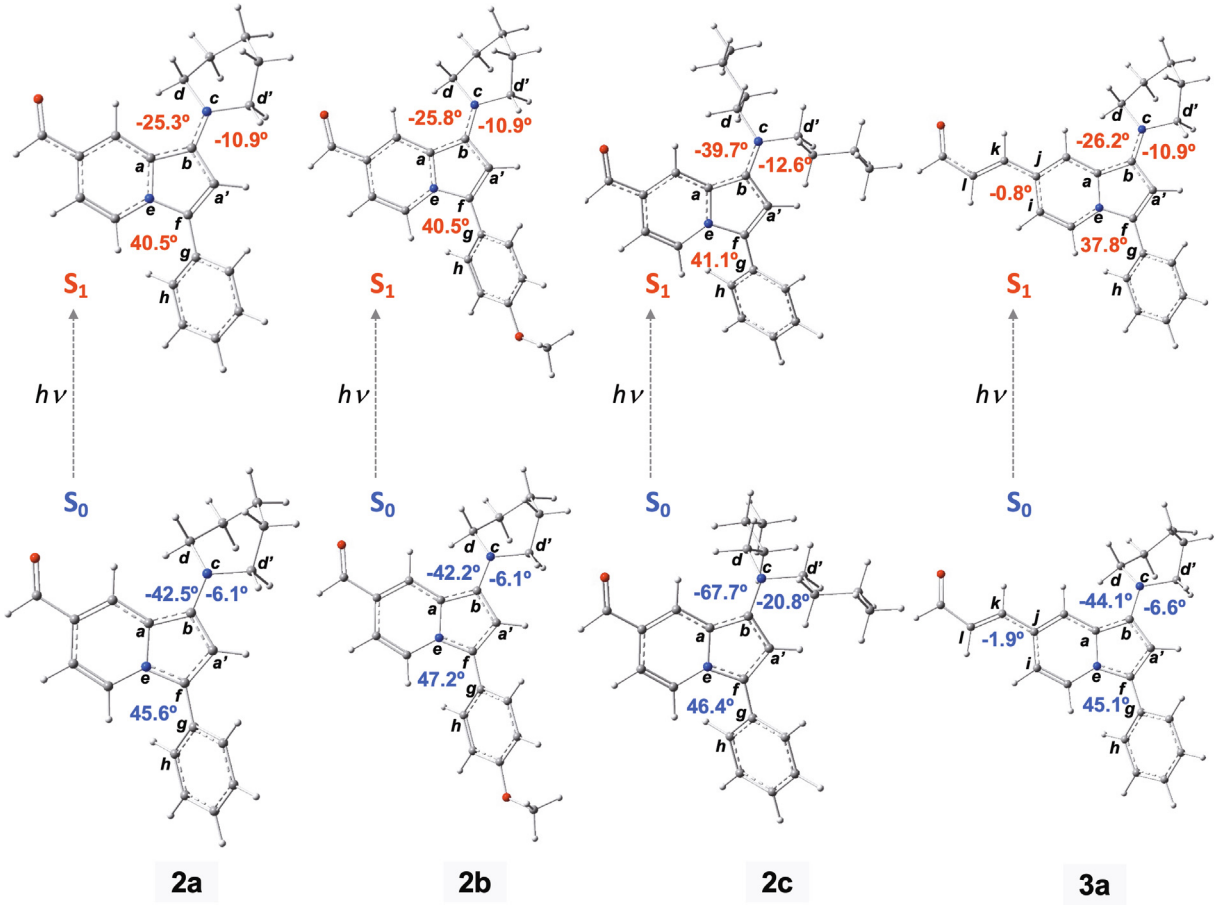

Fig. 4. Selected dihedral angles (in degrees) for the ground (S_0) and excited state (S_1) at the M06-2X/6–31+G** level of theory in CH_2Cl_2 solution. τ_1 (*a,b,c,d*), τ_2 (*a',b,c,d'*), τ_3 (*e,f,g,h*), and τ_4 (*i,j,k,l*).

profile. In this sense, the SS formalism combined with hybrid functionals with high HF% and range-separated functionals may probably be the best strategy for reliable results. Fig. 5 shows the S_1 PES profile of **2a** in CH_2Cl_2 at the TD-M06-2X/6–31+G** level of theory using the cLR and SS formalisms for comparison. The initial molecular geometry for the S_1 state was that in which τ_1 was approximately –25° (PICT) and then the amino group was rotated relative to the indolizine nucleus (TICT around –90°). There is a stabilization of the PICT state with respect to TICT state. In principle, the greater stabilization of the PICT state would not justify the low emissive character of this compound in CH_2Cl_2 solution, with a quantum yield of around 6%. Therefore, the contribution of non-radiative vibrational relaxation could be a mechanism to consider in electronic relaxation (see below).

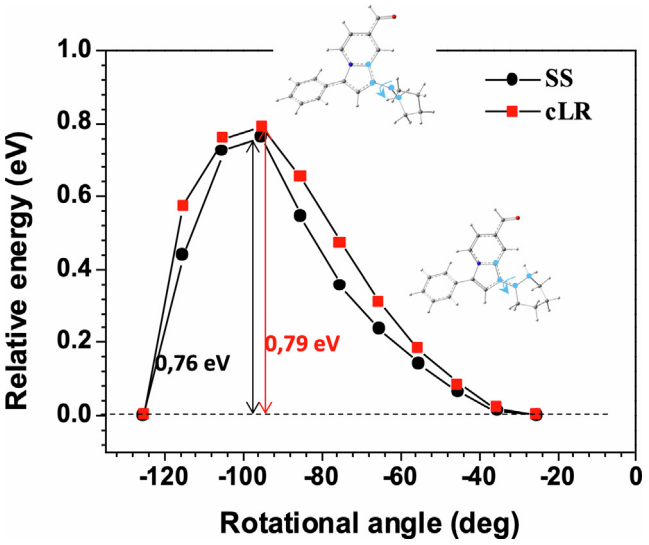

Fig. 5. Energy barrier of S_1 versus rotational angle of **2a** using the cLR and SS formalism calculated at the TD-M06-2X/6–31+G** level of theory in CH_2Cl_2 solution.

Table 3 lists the theoretical emission and oscillator strength (*f*) for the electronic vertical transitions calculated at the M06-2X/6–31+G** level of theory in CH_2Cl_2 solution. There is a good agreement between experimental and theoretical values with differences around 0.1–0.2 eV. The Huang-Rhys factors (HR) were calculated to quantify the non-radiative vibrational relaxation from the excited state (see Table S3). Fig. 6 shows that the largest values were calculated for compound **2c** with HR = 8.1, for the vibrational mode associated to the twisting of the butylamino group calculated at 16 cm^{-1}. For the rest of compounds, the HR values were around 1–2.5, involving the twisting of the piperidinyl group and also of the aryl ring. The branched nature of the dibutylamino group compared to the cyclic nature of the piperidinyl group could favor a greater vibrational relaxation in the first case. On the other hand, the sum of the HR factors is 24.0 for compound **2c**, while for **2a**, **2b**, and **3a** it is 6.3, 6.2, and 14.4, respectively. Despite these differences, similar small quantum yields were measured for all compounds, which suggests that vibrational relaxation is not the only non-radiative relaxation pathway.

2.3. Effect of protonation

The photophysical study was also performed on a 10^{-2} M solution of trifluoroacetic acid (TFA) in CH_2Cl_2 (Table 2). A hypsochromic shift of both the absorption and emission bands was observed for all compounds through the protonation of the different pH responsive elements of the structure and, consequently, the reduction of the electron-donating character. It is worth noting that the acidified solutions emitted blue-cyan light with higher ϕ_F than the neutral counterparts. Similar results were obtained in solvents such as *n*-heptane, toluene, and acetonitrile (Table S1). A less extended emission solvatochromic range is observed, indicating that ICT is less important for the protonated forms.

The effect of protonation was studied in more detail by titration of the CH_2Cl_2 solutions with TFA. As an example, the changes observed in the absorption and emission spectra for **2b** are illustrated in Fig. 7.

The UV–vis spectra showed the progressive disappearance of the charge transfer absorption band of the neutral form, whereas a blue-shifted band for the protonated form progressively appeared. The presence of an isosbestic point is evident and this is characteristic of an equilibrium between two species. At low concentration of acid, only the piperidinyl group at position 1 is expected to undergo protonation ($pK_a \sim 10.1$). The same trend was observed in the fluorescence spectra: the progressive disappearance of the emission band of the neutral form was associated with the enhancement of a new blue-shifted band corresponding to the emission of the protonated form. These changes were found to be fully reversible by neutralization with a base such as 1,8-diazabicyclo[5.4.0]undec-7-ene (DBU). A similar behavior was observed for all indolizines **2a-c** and **3a** (see the Supplementary data, Figs. S12-S14). The disappearance of a well-defined isoemissive point at high concentration of acid might be attributed to a significant change in polarity or, most likely, to the loss of stability shown by the protonated compounds upon continuous irradiation, in contrast to the photochemical stability mentioned above in the absence of acid (Figs. S5-S8). The coexistence of diprotonated species by further protonation of the indolizine nucleus ($pK_a \sim 3.9$) is hardly plausible.

The effect of protonation was also studied by ^1H NMR spectroscopy. The gradual addition of TFA to a $CDCl_3$ solution of **2a** resulted in a progressive deshielding of all signals, except those of the phenyl group (Fig. 8). After the addition of 2 equivalents of acid, this deshielding effect was clearly more pronounced for the α-hydrogens to the piperidinyl nitrogen and the β-hydrogen to the formyl group (the δ values are indicated on the molecular structures). This result suggests that the piperidinyl N is protonated at this stage. Protonation breaks the resonance involving the conjugated δ-aminodienecarbaldehyde unit, which makes the electron-withdrawing action of the formyl group on the β-H stronger. A higher amount of TFA affects the aliphatic signals more than the aromatic signals of the compound. According to the literature, the absence of signals at 4.1–4.3 ppm and 5.2–5.6 ppm denotes that there is no protonation at C1 and C3 of the indolizine nucleus, respectively [15a].

The molecular geometry and photophysical properties of the protonated compounds were also calculated at the M06-2X/6–31+G** level of theory in CH_2Cl_2 solution. Tables 2 and 3 collect the wavelength for the vertical electronic transitions and the corre-

Table 3
Experimental maximum emission wavelength (λ_{em}^{exp}) and calculated emission wavelength (λ_{em}^{calc}) for the $S_1 \rightarrow S_0$ transition in CH_2Cl_2 solution calculated at the TD-M06-2X/6–31+G** level of theory.

Compd	λ_{em}^{exp} nm(eV)	Φ_F	λ_{em}^{calc} nm(eV)	*f*	% Contribution
2a	604 (2.05)	0.06	665 (1.87)	0.27	H ← L (96)
2b	607 (2.04)	0.04	666 (1.86)	0.27	H ← L (96)
2c	597 (2.08)	0.06	678 (1.83)	0.25	H ← L (96)
3a	657 (1.89)	0.06	616 (2.01)	0.85	H ← L (96)
			+ TFA		
2aH$^+$	480 (2.58)	0.15	491 (2.53)	0.36	H ← L (97)
2bH$^+$	491 (2.53)	0.07	518 (2.40)	0.40	H ← L (95)
2cH$^+$	476 (2.60)	0.34	491 (2.53)	0.35	H ← L (97)
3aH$^+$	503 (2.46)	0.08	504 (2.46)	1.03	H ← L (95)

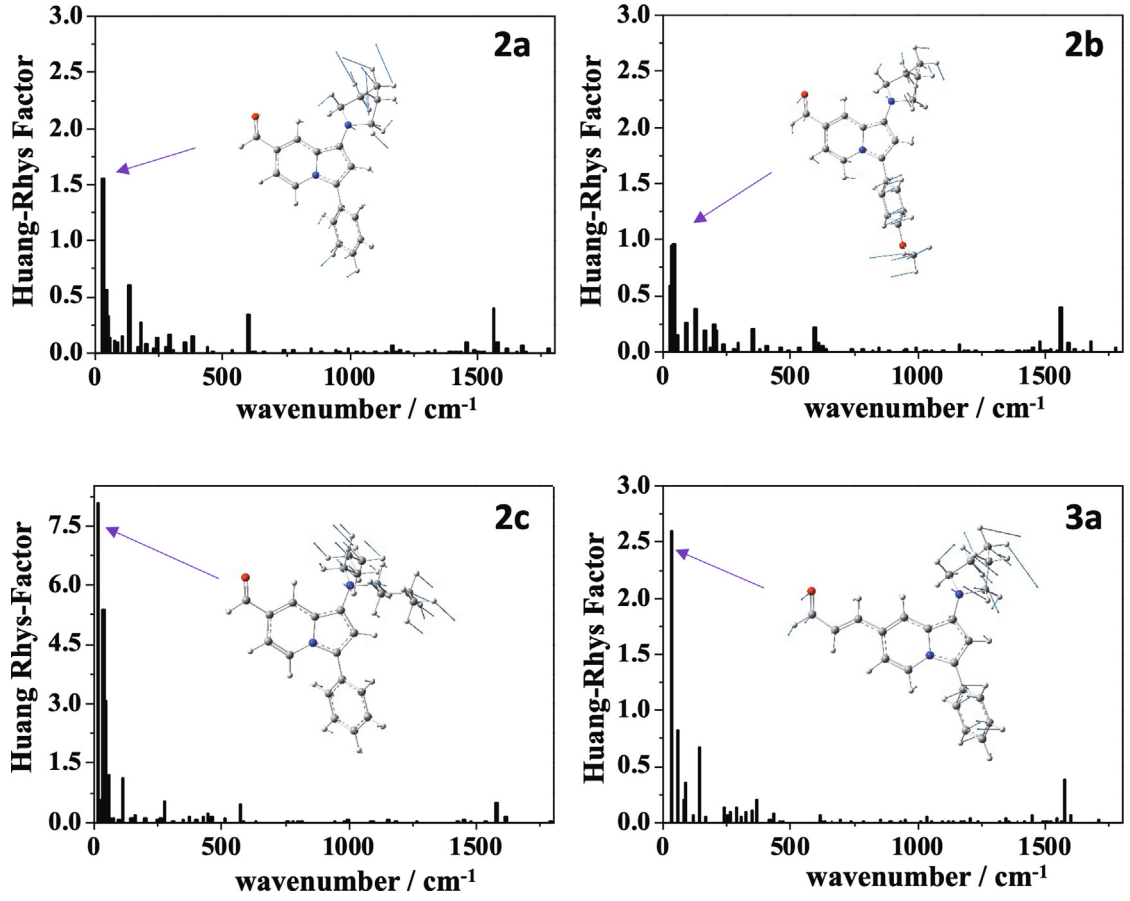

Fig. 6. Huang-Rhys factors *vs.* normal mode wavenumbers (in cm^{-1}) of the ground state calculated for **2a, 2b, 2c**, and **3a** in CH_2Cl_2 solution at the M06-2X/6–31+G** level of theory.

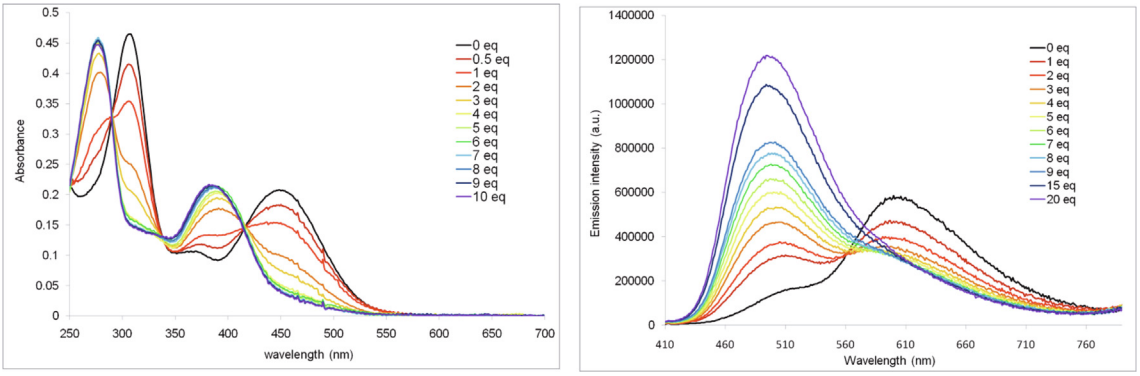

Fig. 7. Changes in the absorption and emission (λ_{exc} = 400 nm) spectra of a CH_2Cl_2 solution of **2b** ($c = 2.2 \times 10^{-5}$ M) upon addition of TFA.

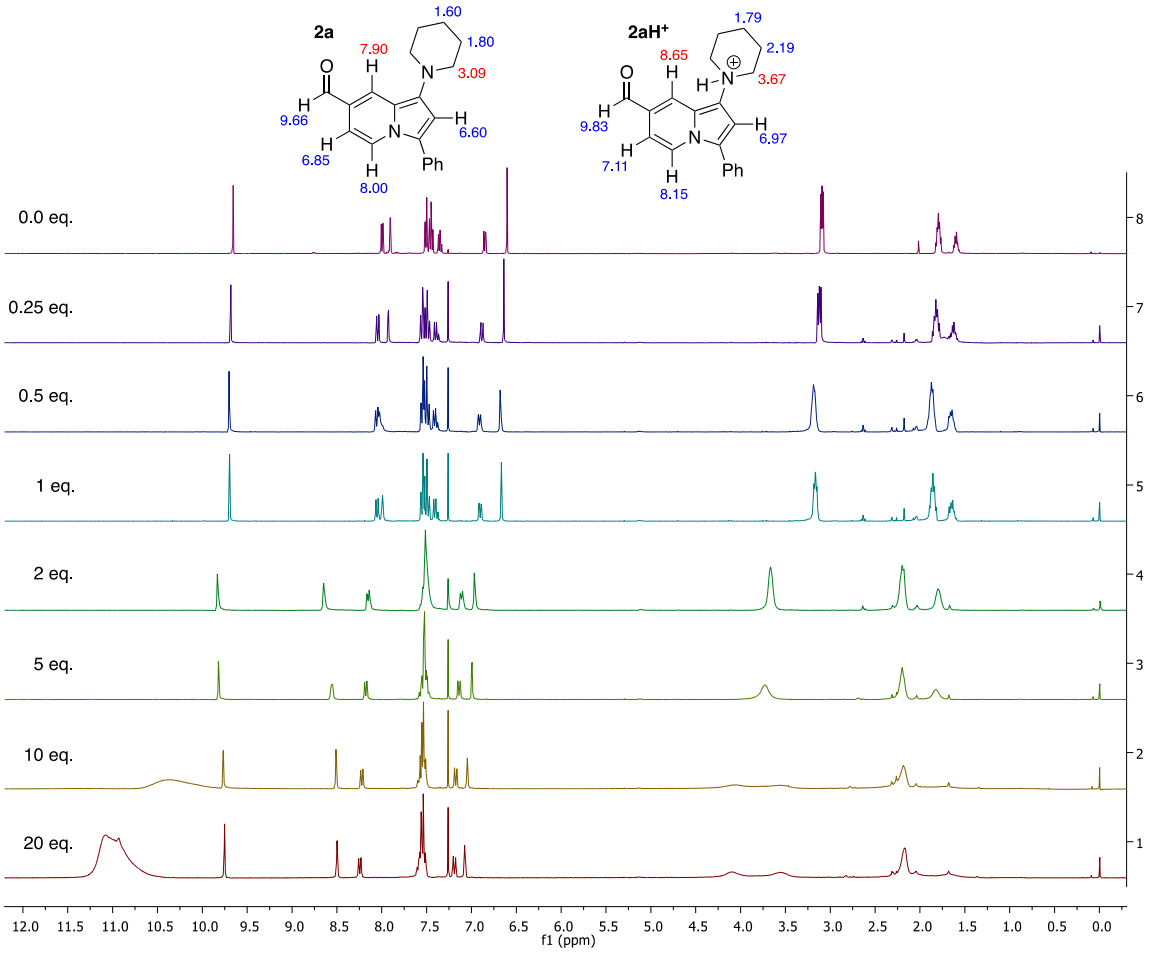

Fig. 8. ^{1}H NMR protonation study on indolizine **2a** by gradual addition of TFA.

sponding oscillator strength. A hypsochromic shift of both absorption and emission transitions was predicted compared with the neutral species along with a higher oscillator strength for the $S_1 \rightarrow S_0$ transition, in agreement with the experimental observations. The large Stokes shifts measured for the protonated species were also due to the significant variation of some dihedral angles upon photoexcitation. Fig. 9 shows some selected dihedral angles for the optimized protonated compounds. As a consequence of the protonation, the amine nitrogen becomes pyramidal (sp^3) and the dihedral angle τ_1 between the amino group and the indolizine nucleus increases significantly (80-94°) compared with the neutral compounds (42-68°). In addition, a significant change is found for τ_3, which decreases 17-22° upon excitation while the variations were only 5-7° for the unprotonated forms. Therefore, the π-conjugation between the indolizine and the aryl ring is increased upon excitation to a greater extent than in the neutral species, favoring the increase of quantum yield. Fig. 10 shows a representation of the frontier molecular orbitals for the protonated compounds. The HOMO is delocalized on both the indolizine nucleus and the aryl ring, while the LUMO is primarily localized on the indolizine. In addition, unlike the neutral species, there is an appreciable decrease of the electron density around the amino group in the HOMO. As a consequence, the ICT would disappear upon excitation. This result is in agreement with the increase in ϕ_F for the protonated species compared with the neutral counterparts.

The Huang-Rhys factors (HR) were also calculated to quantify the non-radiative vibrational relaxation from the excited state (see Table S4). In general, higher HR factors values were predicted for the protonated compounds compared with the neutral species, except for compound **2cH$^+$**. The sum of the HR factors was 17.2, 11.1, and 16.7 for **2aH$^+$**, **2bH$^+$**, and **3aH$^+$**, respectively, whereas a value of 7.3 was obtained for compound **2cH$^+$**. This fact can justify that although the ICT from the amino group to the indolizine decreases, expecting a higher emission with respect to neutral species, the quantum yield increases only slightly due to the greater non-radiative vibrational relaxation (except for **2cH$^+$**). Fig. 11 shows that the largest values were calculated for compound **2aH$^+$** (HR = 7.4) and **3aH$^+$** (HR = 5.3) for the vibrational mode associated to the twisting of the piperidine group calculated at 57 cm^{-1} and 67 cm^{-1}, respectively. For the rest of compounds, several modes with HR factors around 1.5–2.6 were predicted, involving the twisting of both the amino group and the aryl ring. The lowest contribution to the vibrational relaxation was found for compound **2cH$^+$**, in agreement with the largest increase in quantum yield after protonation (from 6% to 34%, Table 1).

The coexistence of both neutral and protonated species with complementary emitting colors in the solution enabled white light emission to be achieved under UV irradiation. Thus, a 2.2×10^{-5} M solution of **2b** in CH_2Cl_2 emitted orange light at λ_{max} = 605 nm and this turned to cyan at λ_{max} = 491 nm upon protonation. Excitation at 400 nm led to the obtention of white light after the addition of 5 equivalents of TFA. The change in the emission color could be easily seen with the naked eye, as shown in Fig. 12. Except for **3a**, the same phenomenon was also observed for all other compounds, obtaining chromaticity coordinates close to those of pure

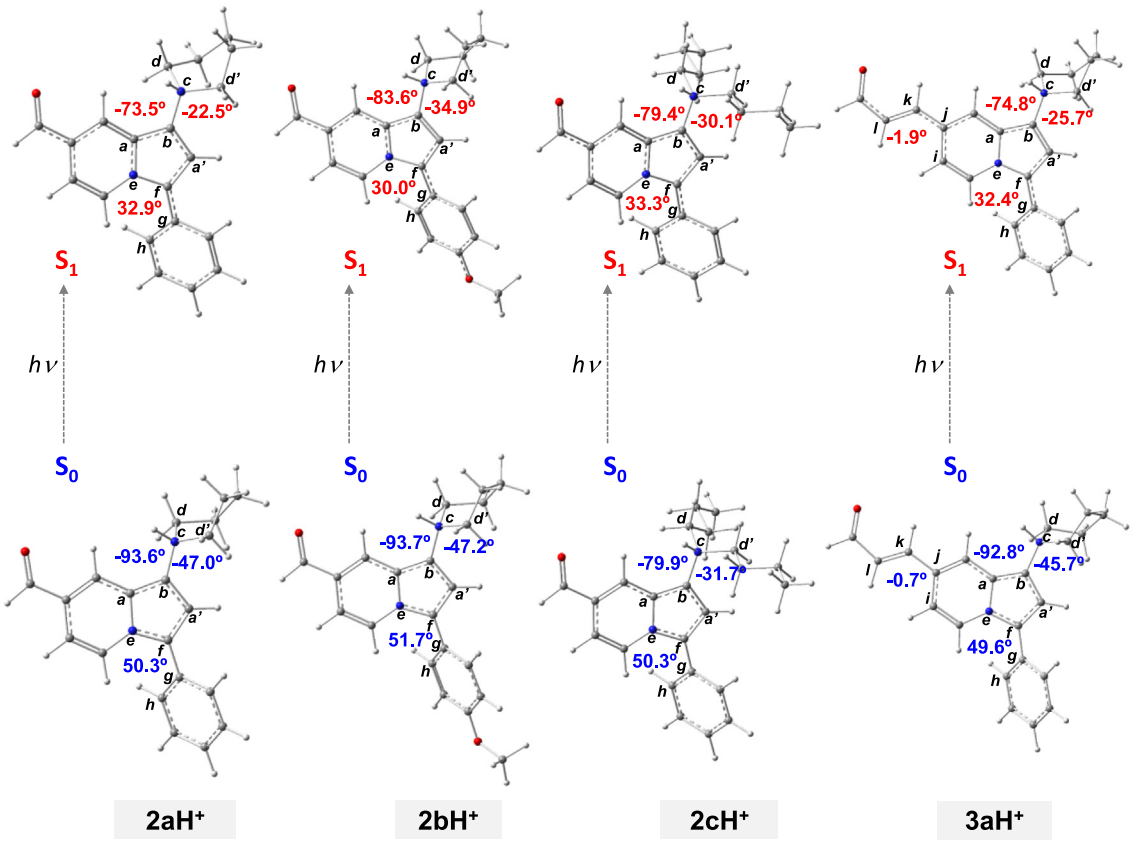

Fig. 9. Selected dihedral angles (in degrees) for the ground S_0 and excited state S_1 of **2aH$^+$**, **2bH$^+$**, **2cH$^+$**, and **3aH$^+$** at the M06-2X/6–31+G** level of theory in CH_2Cl_2 solution. τ_1 (*a,b,c,d*), τ_2 (*a',b,c,d'*), τ_3 (*e,f,g,h*), and τ_4 (*i,j,k,l*).

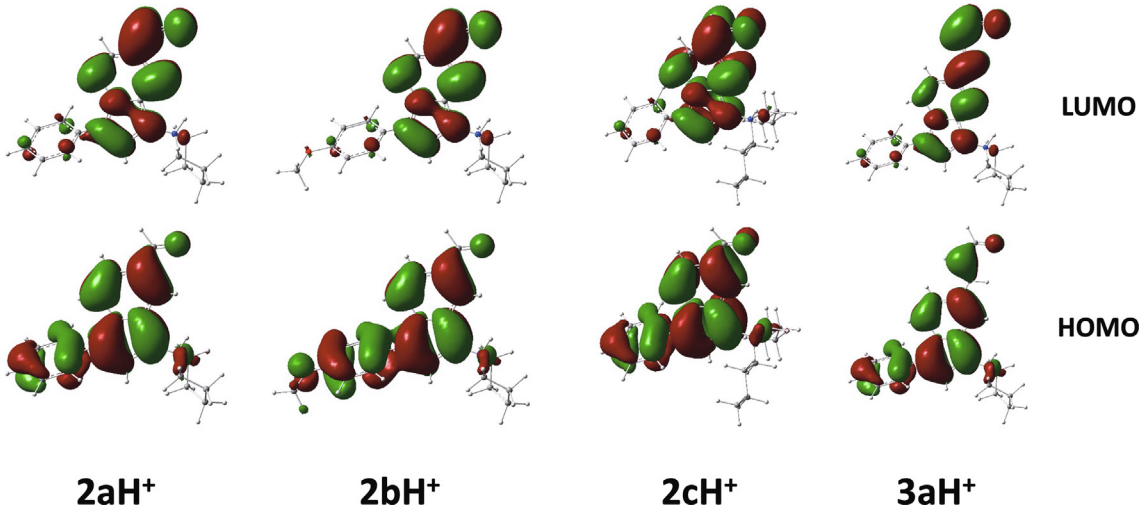

Fig. 10. HOMO and LUMO molecular orbitals (isocontour plots 0.02 a.u.) calculated for **2aH$^+$, 2bH$^+$, 2cH$^+$**, and **3aH$^+$** at the M06-2X/6–31+G** level of theory in CH_2Cl_2 solution (see energy levels in Table S2).

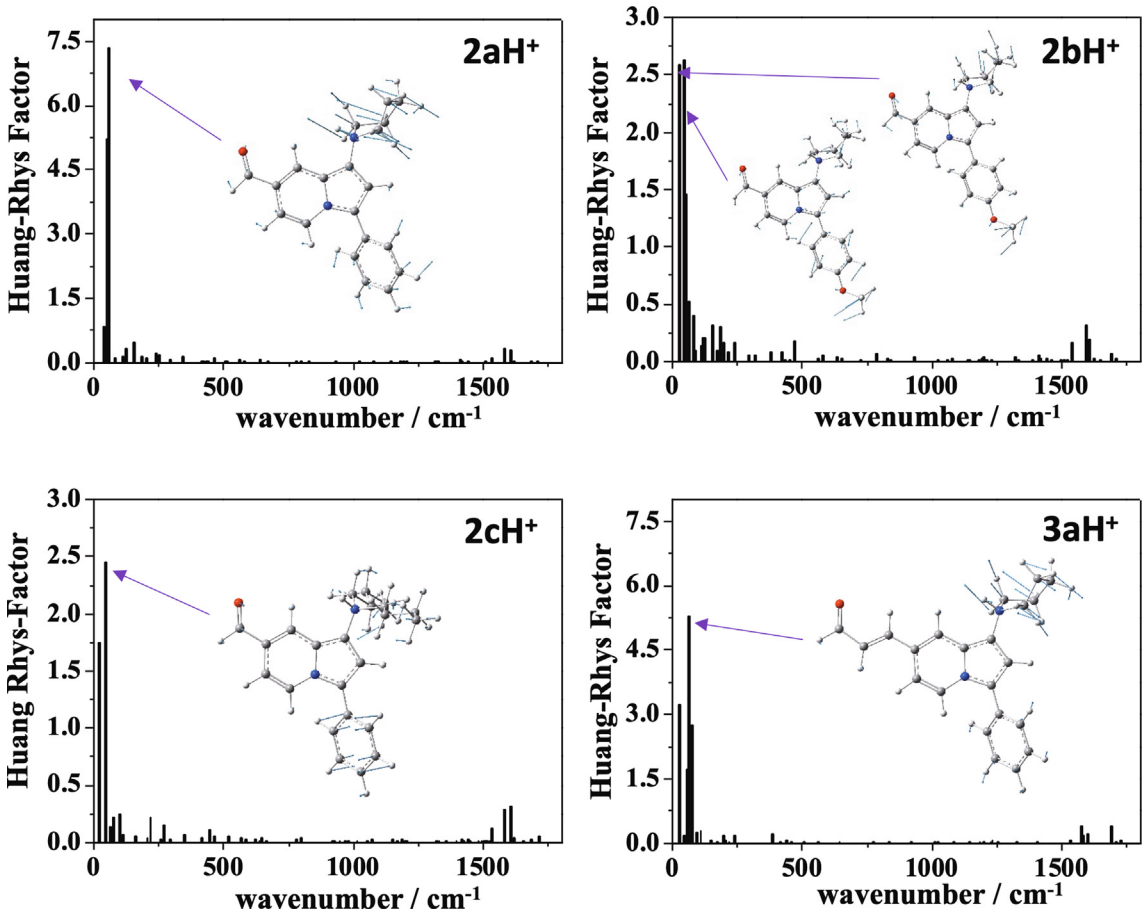

Fig. 11. Huang-Rhys factors *vs.* normal mode wavenumbers (in cm^{-1}) of the ground state calculated for **2aH$^+$**, **2bH$^+$**, **2cH$^+$**, and **3aH$^+$** in CH_2Cl_2 solution at the M06-2X/6–31 +G** level of theory.

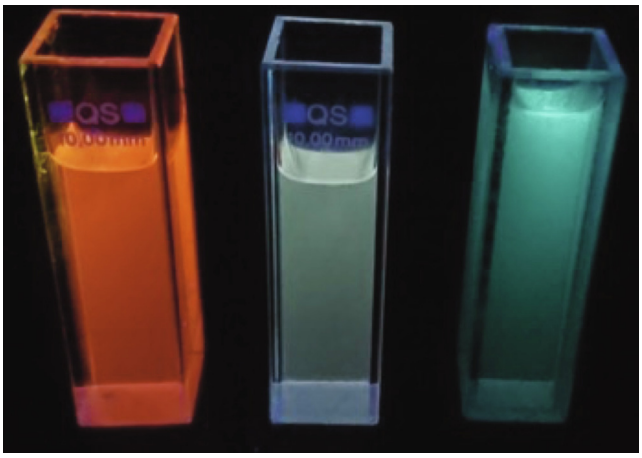

Fig. 12. Changes in the color of a CH_2Cl_2 solution of **2b** (c = 2.2 × 10^{-5} M) after addition of 0 (left), 3 (middle), and 20 equivalents (right) of TFA. Photographs were taken in the dark upon irradiation with a hand-held UV lamp (365 nm).

white light (Table 4, Figs. S15-S17 of the Supplementary data). Controlled protonation is an efficient way to attain a mixture of species with complementary emitting colors in the appropriate ratio to ultimately grant access to white light photoluminescence [3].

Table 4
CIE coordinates in CH_2Cl_2 solution (c = 1.6–2.2 × 10^{-5} M).

Compd	Chromaticity coordinates (x,y)		
	Neutral form	Protonated form	Mixture of neutral and protonated forms
2a	(0.58, 0.41)	(0.22, 0.33)	(0.34, 0.36)[a]
2b	(0.57, 0.42)	(0.24, 0.41)	(0.32, 0.43)[b]
2c	(0.55, 0.43)	(0.21, 0.27)	(0.32, 0.30)[c]
3a	(0.64, 0.36)	(0.28, 0.46)	(0.32, 0.47)[d]

[a] 30 equiv. of TFA, λ_{exc} = 400 nm. [b] 5 equiv. of TFA, λ_{exc} = 400 nm. [c] 4 equiv. of TFA, λ_{exc} = 400 nm. [d] 100 equiv. of TFA, λ_{exc} = 430 nm.

3. Conclusions

A series of trisubstituted indolizines bearing 1-amino, 3-aryl, and 7-formyl groups have been synthesized by regioselective formylation of the parent 1,3-disubstituted indolizines, using the Eschenmoser's salt as a formylation agent. The conjugation of one of them has been further extended by condensation with acetone. All indolizines are push–pull chromophores that exhibit selective protonation at the amino group, as demonstrated by ^{1}H NMR titration. Contrary to what is generally observed for push–pull π-deficient azaheterocycles upon protonation (i.e., bathochromic shift in the emission curves), the protonation of the 1-amino group in the mentioned indolizines leads to a hypsochromic shift in the emission spectra. Furthermore, white photoluminescence could be achieved through a precise control of the amount of acid added, as a consequence of chromatic complementarity in the

emission of the neutral and protonated species. In addition, Density Functional Theory (DFT) calculations in CH_2Cl_2 solution at the M06-2X/6–31+G** level of theory performed on the neutral and protonated species support the hypsochromic shift of both the absorption and emission transitions, according to what was observed experimentally. The relatively large Stokes shifts recorded for the protonated species have been rationalized in terms of the variation of some dihedral angles by photoexcitation. The results of this study underpin controlled protonation in push–pull dyes as one of the avenues to accomplish challenging white light photoluminescence.

4. Experimental section

4.1. General

All the indolizines in this study were prepared as described elsewhere by some of us [19,20]. Compound preparation procedures and their analytical and spectroscopic characterization are given in the Supplementary data. UV–visible and fluorescence spectroscopy studies in solution were conducted on a Spex Fluoromax-3 Jobin-Yvon Horiba spectrofluorometer. All solutions were measured with optical densities below 0.1. Fluorescence quantum yields were determined relative to 9,10-bis(phenylethynyl)anthracene in cyclohexane (ϕ_F = 1.00) [22]. Quartz cuvettes (10 mm, Hellma Analytics) were employed for all spectroscopic measurements.

4.2. Computational details

Full geometry optimization of the ground and first excited state was performed using the Gaussian 16 (revision A.03) suite of programs [27] at the M06-2X/6–31+G** level of theory [28]. The vibrational frequencies were computed to check that all are real. The solvent was treated implicitly using the Polarizable Continuum Model (PCM) [29]. The vertical electronic transitions (absorption and emission) were computed using Time-Dependent DFT calculations (TD-M06-2X/6–31+G**) in CH_2Cl_2 solution. The vertical electronic transition for the emission was calculated as ΔE_{em} = E(S1//S1) - E(S0//S1) where E(S1//S1) is the energy of the S_1 excited state at its equilibrium geometry (state-specific solvation approach) [30] and E(S0//S1) is the energy of the S_0 ground state at the S_1 excited state geometry and with the static solvation from the excited state [31]. The vibrational reorganization energy associated to the non-radiative relaxation of excited electronic states, λ, was computed using the program DUSHIN [32] according to: $\lambda = \sum_i \lambda_i = \sum_i \hbar\omega_i S_i$. ω_i is the wavenumber associated to the vibrational mode i which assists the internal conversion process, and S_i is the dimensionless Huang-Rhys (HR) factor calculated from the atomic displacements (ΔQ), and force constant (k), of the normal mode i according to $S_i = \frac{1}{2} k \frac{\Delta Q^2}{\hbar\omega_i}$. The S_1 relaxed potential energy curve was calculated in CH_2Cl_2 solution as a function of the rotational angle between the piperidinyl moiety and the indolizine platform at the TD-M06-2X/6–31+G** level of theory. Geometry optimizations were made at each point using the LR formalism. Then, corrected linear-response (cLR) and state-specific (SS) single-points were computed on this LR-relaxed scan. The dihedral angle was changed by 10° in each step while the other geometry parameters were freely relaxed.

CRediT authorship contribution statement

Teresa Antón-Cánovas: Investigation, Data curation. **Sylvain Achelle:** Conceptualization, Investigation, Methodology, Resources, Supervision, Writing – review & editing. **M. Paz Fernández-Liencres:** Investigation, Data curation, Methodology, Software. **Amparo Navarro:** Conceptualization, Funding acquisition, Methodology, Resources, Software, Supervision, Writing – original draft, Writing – review & editing. **Francisco Alonso:** Conceptualization, Funding acquisition, Methodology, Resources, Supervision, Writing – original draft, Writing – review & editing. **Julián Rodríguez-López:** Conceptualization, Funding acquisition, Methodology, Resources, Supervision, Writing – original draft, Writing – review & editing.

Declaration of Competing Interest

The authors declare that they have no known competing financial interests or personal relationships that could have appeared to influence the work reported in this paper.

Acknowledgments

This work was supported by Spanish Ministerio de Ciencia e Innovación (project CTQ2017-88171-P), Generalitat Valenciana (projects AICO/2017/007 and APOTIP/2021/018), Vicerrectorado de Investigación–Universidad de Alicante (grant UAFPU20-02 for T.A.-C.), Instituto de Síntesis Orgánica (ISO)–Universidad de Alicante, Junta de Comunidades de Castilla-La Mancha/FEDER (project SBPLY/21/180501/000042), Junta de Andalucía (FQM-337), and Universidad de Jaén–FEDER/UJA/2020 (project 2021/00627/001). The Centro de Servicios de Informática y Redes de Comunicaciones (CSIRC, Universidad de Granada) was instrumental in providing the computer time that made this work possible.

Appendix A. Supplementary data

Supplementary data to this article can be found online at https://doi.org/10.1016/j.molliq.2023.121758.

References

[1] O. Ostroverkhova, Organic optoelectronic materials: mechanisms and applications, Chem. Rev. 116 (2016) 13279–13412, https://doi.org/10.1021/acs.chemrev.6b00127.
[2] F. Bureš, Fundamental aspects of property tuning in push–pull molecules, RSC Adv. 4 (2014) 58826–58851, https://doi.org/10.1039/C4RA11264D.
[3] S. Achelle, J. Rodríguez-López, F. Bureš, F. Robin-le Guen, Tuning the photophysical properties of push-pull azaheterocyclic chromophores by protonation: a brief overview of a French-Spanish-Czech project, Chem. Rec. 20 (2020) 440–451, https://doi.org/10.1002/tcr.201900064.
[4] (a) M.D. Smith, H.I. Karunadasa, White-light emission from layered halide perovskites, Acc. Chem. Res. 51 (2018) 619–627. . (b) D. Cortecchia, J. Yin, A. Petrozza, C. Soci, White light emission in low-dimensional perovskites, J. Mater. Chem. C 7 (2019) 4956–4969. https://doi.org/10.1039/C9TC01036J. (c) F. Li, X. Li, Y. Wang, X. Zhang, Trismaleimide dendrimers: helix-to-superhelix supramolecular transition accompanied by white-light emission, Angew. Chem. Int. Ed. 58 (2019) 17994–18002. https://doi.org/10.1002/anie.201908837. (d) Z. Wang, C.-Y. Zhu, J.-T. Mo, P.-Y. Fu, Y.-W. Zhao, S.-Y. Yin, J.-J. Jiang, M. Pan, C.-Y. Su, White-Light emission from dual-way photon energy conversion in a dye-encapsulated metal-organic framework, Angew. Chem. Int. Ed. 58 (2019) 9752-9757. https://doi.org/10.1002/anie.201905186https://doi.org/10.1002/anie.201905186. (e) N.-C. Chiu, K.T. Smith, K.C. Stylianou, Metal-organic frameworks for white light emission: from synthesis to device fabrication, Coord. Chem. Rev. 459 (2022) 214441. https://doi.org/10.1016/j.ccr.2022.214441.
[5] B. Sadowski, J. Klajn, D.T. Gryko, Recent advances in the synthesis of indolizines and their π-expanded analogues, Org. Biomol. Chem. 14 (2016) 7804–7828, https://doi.org/10.1039/C6OB00985A.
[6] A. Brandi, S. Cicchi, F.M. Cordero, Bicyclic 5-6 systems with one bridgehead (ring junction) nitrogen atom: no extra heteroatom, in: D.StC. Black, J. Cossy, C. V. Stevens (Eds.), Comprehensive Heterocyclic Chemistry IV, Elsevier, Oxford, 2022, Vol. 11, Chap. 11.08, pp. 437–527. https://doi.org/10.1016/B978-0-12-409547-2.14938-8.
[7] (a) G.L. Fletcher, Jr., S.L. Bender, D.H. Wadsworth (Eastman Kodak Co.), Eur. Pat. 68876A1, 1983; Chem. Abstr. 100 (1984) 122772. (b) Y. Inagaki, K. Adachi, M. Yabe (Fuji Photo Film Co., Ltd.), Jap. Pat. 02062280A, 1990; Chem. Abstr. 114 (1991) 52945. (c) A. Takazawa, T. Kobayashi (Fuji Photo Film Co., Ltd.), Jap. Pat. 03113847A, 1991; Chem. Abstr. 115 (1991) 267063. (d) T. Suzuki, M. Shinkai, N. Nanba (TDK Electronics Co., Ltd.), Jap. Pat. 07126543A, 1995; Chem. Abstr. 123 (1995), 183678.

[8] Y. Inagaki, T. Kubo (Fuji Photo Film Co., Ltd.), Jap. Pat. 03074471A, 1991; Chem. Abstr. 115 (1991) 138212.
[9] Y.-S. Jung, J.-Y. Jaung, Halochromism of pyridinium azomethine ylides stabilized by dicyanopyrazine group, Dyes Pigm. 65 (2005) 205–209, https://doi.org/10.1016/j.dyepig.2004.07.020.
[10] J. Tanabe, M. Shinkai, M. Tsuchiya (TDK Electronics Co., Ltd.), Jap. Pat. 2008101064A, 2008; Chem. Abstr. 148 (2008) 520703.
[11] (a) M.F.Z.J. Amaral, L.A. Deliberto, C.R. de Souza, R.M.Z.G. Naal, Z. Naal, G.C. Clososki, Synthesis, photophysical, and electrochemical properties of 2,5-diarylindolizines, Tetrahedron 70 (2014) 3249–3252. https://doi.org/10.1016/j.tet.2013.11.105. (b) Y.R. Song, C.W. Lim, T.W. Kim, Synthesis and photophysical properties of 1,2-diphenylindolizine derivatives: fluorescent blue-emitting materials for organic light-emitting device, Luminescence 31 (2016) 364–371. https://doi.org/10.1002/bio.2968. (c) Y. Zhang, J. Garcia-Amorós, B. Captain, F.M. Raymo, A fluorescent and halochromic indolizine switch, J. Mater. Chem. C 4 (2016) 2744–2747. https://doi.org/10.1039/C5TC03331D. (d) V.K. Outlaw, J. Zhou, A.E. Bragg, C.A. Townsend, Unusual blue-shifted acid-responsive photoluminescence behavior in 6-amino-8-cyanobenzo[1,2-*b*]indolizines, RSC Adv. 6 (2016) 61249–61253. https://doi.org/10.1039/C6RA10605F. (e) T. Kim, J. Kim, Color-tunable indolizine-based fluorophores and fluorescent pH sensor, Molecules 27 (2022) 12. https://doi.org/10.3390/molecules27010012. (e) C.R.S. Bertallo, L.S. Berlim, D.S. Olivier, T. R. Arroio, A.S. Ito, G.C. Clososki, Synthesis and photophysical properties of 2-aryl-5-carbonyl indolizines, Dyes Pigm. 198 (2022) 109996. https://doi.org/10.1016/j.dyepig.2021.109996. (f) J.S.A. Badaro, B. Koszarna, M.H.E. Bousquet, E.T. Ouellette, D. Jacquemin, D.T. Gryko, The Kröhnke synthesis of benzo[*a*]indolizines revisited: towards small, red light emitters, Org. Chem. Front. 9 (2022) 1861–1874. https://doi.org/10.1039/D2QO00097K.
[12] (a) B. Liu, Z. Wang, N. Wu, M. Li, J. You, J. Lan, Discovery of a full-color-tunable fluorescent core framework through direct C-H (hetero)arylation of N-heterocycles, Chem. Eur. J. 18 (2012) 1599–1603. https://doi.org/10.1002/chem.201103329. (b) E. Kim, Y. Lee, S. Lee, S.B. Park, Discovery, understanding, and bioapplication of organic fluorophore: a case study with an indolizine-based novel fluorophore, Seoul-Fluor, Acc. Chem. Res. 48 (2015) 538−547. https://doi.org/10.1021/ar500370v.
[13] A.J. Huckaba, F. Giordano, L.E. McNamara, K.M. Dreux, N.I. Hammer, G.S. Tschumper, S.M. Zakeeruddin, M. Grätzel, M.K. Nazeeruddin, J.H. Delcamp, Indolizine-based donors as organic sensitizer components for dye-sensitized solar cells, Adv. Energy Mater. 5 (2015) 1401629, https://doi.org/10.1002/aenm.201401629.
[14] (a) Z.I.M. Allaoui, E. le Gall, A. Fihey, R. Plaza-Pedroche, C. Katan, F. Robin-le Guen, J. Rodríguez-López, S. Achelle, Push-pull (iso)quinoline chromophores: synthesis, photophysical properties, and use for white-light emission, Chem. Eur. J. 26 (2020) 8153–8161. https://doi.org/10.1002/chem.202000817. (b) T. Sachdeva, S. Gupta, M.D. Milton, Smart organic materials with acidochromic properties, Curr. Org. Chem. 24 (2020) 1976–1998 https://doi.org/10.2174/1385272824999200729132853.
[15] (a) W.L.F. Armarego, C-1 and C-3 protonation of indolizines, J. Chem. Soc. B (1966) 191–194. . (b) K.M. Elattar, I. Youssef, A.A. Fadda, Reactivity of indolizines in organic synthesis, Synth. Commun. 46 (2016) 719–744. https://doi.org/10.1080/00397911.2016.1166252.
[16] E. Kim, S. Lee, S.B. Park, 9-Aryl-1,2-dihydropyrrolo[3,4-*b*]indolizin-3-one (Seoul-Fluor) as a smart platform for colorful ratiometric fluorescent pH sensors, Chem. Commun. 47 (2011) 7734–7736, https://doi.org/10.1039/c1cc12618k.
[17] (a) M.J. Albaladejo, M.J. González-Soria, F. Alonso, Synthesis of aminoindolizidines through the chemoselective and diastereoselective catalytic hydrogenation of indolizines, J. Org. Chem. 81 (2016) 9707–9717. https://doi.org/10.1021/acs.joc.6b01782. (b) M.J. González-Soria, F. Alonso, Substrate-controlled divergent synthesis of enaminones and pyrroles from indolizines and nitroso compounds, Adv. Synth. Catal. 361 (2019) 5005-5017. https://doi.org/10.1002/adsc.201900837.
[18] (a) F. Alonso Valdés, M.J. Albaladejo Maricó (Universidad de Alicante), Indolizines with dye properties and method for the synthesis of said indolizines. WO 2015/097328, 2015. (b) M.J. Albaladejo, M.J. González-Soria, F. Alonso, Metal-free remote-site C–H alkenylation: regio- and diastereoselective synthesis of solvatochromic dyes, Green Chem. 20 (2018) 701–712. https://doi.org/10.1039/C7GC03436A.
[19] M.J. Albaladejo, F. Alonso, M.J. González-Soria, Synthetic and mechanistic studies on the solvent-dependent copper-catalyzed formation of indolizines and chalcones, ACS Catal. 5 (2015) 3446–3456, https://doi.org/10.1021/acscatal.5b00417.
[20] (a) T. Antón-Cánovas, F. Alonso (Universidad de Alicante), Formylation of indolizines and detection of nitrites. WO 2021/250296, 2021. (b) T. Antón-Cánovas, F. Alonso, The Eschenmoser's salt as a formylation agent for the synthesis of indolizinecarbaldehydes and their use for colorimetric nitrite detection. Angew. Chem. Int. Ed. 62 (2023) e202215916. https://doi.org/10.1002/anie.202215916.
[21] W. Flitsch, Bicyclic 5-6 systems with one ring junction nitrogen atom: no extra heteroatom, in: A.R. Katrizky, C.W. Rees, E.F.V. Scriven, G. Jones (Eds.), Comprehensive Heterocyclic Chemistry II, Pergamon, Exeter, 1996, Vol. 8, Chap. 8.09, pp. 1–24. https://doi.org/10.1016/B978-008096518-5.00168-4.
[22] M. Taniguchi, J.S. Lindsey, Database of absorption and fluorescence spectra of >300 common compounds for use in PhotochemCAD, Photochem. Photobiol. 94 (2018) 290–327, https://doi.org/10.1111/php.12860.
[23] R. Lartia, C. Allain, G. Bordeau, F. Schmidt, C. Fiorini-Debuisschert, F. Charra, M.-P. Teulade-Fichou, Synthetic strategies to derivatizable triphenylamines displaying high two-photon absorption, J. Org. Chem. 73 (2008) 1732–1744, https://doi.org/10.1021/jo702002y.
[24] X. Liu, Q. Qiao, W. Tian, W. Liu, J. Chen, M.J. Lang, Z. Xu, Aziridinyl fluorophores demonstrate bright fluorescence and superior photostability by effectively inhibiting twisted intramolecular charge transfer, J. Am. Chem. Soc. 138 (2016) 6960–6963, https://doi.org/10.1021/jacs.6b03924.
[25] C.A. Guido, B. Mennucci, D. Jacquemin, C. Adamo, Planar *vs.* twisted intramolecular charge transfer mechanism in Nile Red: new hints from theory, Phys. Chem. Chem. Phys. 12 (2010) 8016–8023, https://doi.org/10.1039/b927489h.
[26] C. Wang, Q. Qiao, W. Chi, J. Chen, W. Liu, D. Tan, S. McKechnie, D. Lyu, X.-F. Jiang, W. Zhou, N. Xu, Q. Zhang, Z. Xu, X. Liu, Quantitative design of bright fluorophores and AIEgens by the accurate prediction of twisted intramolecular charge transfer (TICT), Angew. Chem. Int. Ed. 59 (2020) 10160–10172, https://doi.org/10.1002/anie.201916357.
[27] Gaussian 16, Revision A.03. M.J. Frisch, G.W. Trucks, H.B. Schlegel, G.E. Scuseria, M.A. Robb, J.R. Cheeseman, G. Scalmani, V. Barone, G.A. Petersson, H. Nakatsuji, X. Li, M. Caricato, A.V. Marenich, J. Bloino, B.G. Janesko, R. Gomperts, B. Mennucci, H.P. Hratchian, J.V. Ortiz, A.F. Izmaylov, J.L. Sonnenberg, D. Williams-Young, F. Ding, F. Lipparini, F. Egidi, J. Goings, B. Peng, A. Petrone, T. Henderson, D. Ranasinghe, V.G. Zakrzewski, J. Gao, N. Rega, G. Zheng, W. Liang, M. Hada, M. Ehara, K. Toyota, R. Fukuda, J. Hasegawa, M. Ishida, T. Nakajima, Y. Honda, O. Kitao, H. Nakai, T. Vreven, K. Throssell, J.A. Montgomery, Jr., J.E. Peralta, F. Ogliaro, M.J. Bearpark, J.J. Heyd, E.N. Brothers, K.N. Kudin, V.N. Staroverov, T.A. Keith, R. Kobayashi, J. Normand, K. Raghavachari, A.P. Rendell, J.C. Burant, S.S. Iyengar, J. Tomasi, M. Cossi, J.M. Millam, M. Klene, C. Adamo, R. Cammi, J.W. Ochterski, R.L. Martin, K. Morokuma, O. Farkas, J.B. Foresman, D.J. Fox, Gaussian, Inc., Wallingford CT, 2016.
[28] Y. Zhao, D.G. Truhlar, The M06 suite of density functionals for main group thermochemistry, thermochemical kinetics, noncovalent interactions, excited states, and transition elements: two new functionals and systematic testing of four M06-class functionals and 12 other functionals, Theor. Chem. Acc. 120 (2008) 215–241, https://doi.org/10.1007/s00214-007-0310-x.
[29] (a) M. Cossi, N. Rega, G. Scalmani, V. Barone, Energies, structures, and electronic properties of molecules in solution with the C-PCM solvation model, J. Comput. Chem. 24 (2003) 669−681. https://doi.org/10.1002/jcc.10189. (b) J. Tomasi, B. Mennucci, R. Cammi, Quantum mechanical continuum solvation models, Chem. Rev. 105 (2005) 2999–3094. https://doi.org/10.1021/cr9904009. (c) R. Cammi, S. Corni, B. Mennucci, J. Tomasi, Electronic excitation energies of molecules in solution: state specific and linear response methods for nonequilibrium continuum solvation models, J. Chem. Phys. 122 (2005) 104513. https://doi.org/10.1063/1.1867373.
[30] R. Improta, V. Barone, G. Scalmani, M.J. Frisch, A state-specific polarizable continuum model time dependent density functional theory method for excited state calculations in solution, J. Chem. Phys. 125 (2006), https://doi.org/10.1063/1.2222364.
[31] G. Scalmani, M.J. Frisch, B. Mennucci, J. Tomasi, R. Cammi, V. Barone, Geometries and properties of excited states in the gas phase and in solution: theory and application of a time-dependent density functional theory polarizable continuum model, J. Chem. Phys. 124 (2006), https://doi.org/10.1063/1.2173258.
[32] J.R. Reimers, A practical method for the use of curvilinear coordinates in calculations of normal-mode-projected displacements and Duschinsky rotation matrices for large molecules, J. Chem. Phys. 115 (2001) 9103–9109, https://doi.org/10.1063/1.1412875.